Available online at www.sciencedirect.com
SCIENCE DIRECT®
Planetary and Space Science 52 (2004) 199–213
Planetary and Space Science
www.elsevier.com/locate/pss

Insights on rock abrasion and ventifact formation from laboratory and field analog studies with applications to Mars

Nathan T. Bridges[a,*], Julie E. Laity[b], Ronald Greeley[c], James Phoreman[c,1], Eric E. Eddlemon[c,1]

[a] Jet Propulsion Laboratory, MS 183-501, 4800 Oak Grove Drive, Pasadena, CA 91109, USA
[b] Department of Geography, California State University, Northridge, CA 91330, USA
[c] Department of Geological Sciences, Arizona State University, Tempe, AZ 85287-1404, USA

Received 4 March 2003; received in revised form 8 July 2003; accepted 29 August 2003

Abstract

Wind tunnel studies are integrated with field observations to better understand the processes and rates of rock abrasion on Earth and Mars and how these factors affect ventifact morphology. The wind tunnel work consists of controlled experiments at terrestrial and Martian pressures in which known fluxes of sand are blown onto abradable targets of various geometric shapes. Mass loss and dimensional changes are measured and shape evolution observed as a function of total sand flux, wind speed, target shape, and target composition. To provide ground truth to these experiments, the same types of targets were placed in a field plot at a Mojave Desert ventifact locality for 6 months and measurements and observations like those in the wind tunnel were made. Weather data recorded by a co-located station provided wind speed and direction during this time. These data and results from the abraded field targets were compared to flute directions of local ventifacts. Initial results from this work are: (1) initial rock shape controls the rate of abrasion, with steeper faces abrading faster than shallower ones, (2) targets also abrade via slope retreat, with intermediate angled faces becoming shallower (flatter) at a greater rate than initially flat or steep faces, (3) the direction of maximum velocity winds exerts a greater control on ventifact flute orientations than the direction of average velocity winds, (4) irregular targets with pits or grooves abrade at greater rates than targets with smooth surfaces, with indentations generally enlarging and faces becoming rougher with time, and (5) there are many similarities between the experimental and terrestrial ventifacts, as well as rocks interpreted as ventifacts on Mars. The pitted and faceted appearance of many Martian rocks is easily attributable to aeolian abrasion. Many Martian rocks appear pitted or vesicular, characteristics which our laboratory experiments show enhance abrasion. Although measured Martian wind speeds are generally below those necessary to induce saltation, occasional gusts above threshold may be sufficient for some rock abrasion. Ventifact formation is potentially a common geomorphic process on Mars provided there are sufficient supplies of sand and high velocity winds needed for saltation.
© 2003 Elsevier Ltd. All rights reserved.

Keywords: Abrasion; Ventifacts; Surface modification; Aeolian processes; Weathering

1. Introduction

Planetary bodies with sufficiently vigorous wind and mobile surface particles experience aeolian erosion via deflation and abrasion. The former process involves the shearing and turbulent action by near surface winds that remove regolith and poorly cohesive sediments, forming features such as moats, wind tails, and lag deposits at the decimeter scale and may contribute to the development of yardangs at the decameter to 10s of kilometers scale (Ward, 1979; Greeley et al., 1992, 2002). Saltating particles in the lower ~ 1 m of the near-surface boundary layer act to abrade rock surfaces. Given sufficient time, abraded rocks may become pitted, fluted, or grooved. These micro-features are oriented with the direction of predominant winds and thereby serve as proxy data for paleowind directions (Laity, 1994, 1995). Such wind eroded rocks are called ventifacts and give insight into the aeolian regime and climate under which they were modified.

Earth and Mars both possess sand-size particles and atmospheres capable of moving them under optimum conditions. Not surprisingly, it is only on these planets that features associated with deflation and abrasion have so far been found. On Earth, ventifacts, soil deflational features, and yardangs are well documented, being most abundant in

* Corresponding author. Tel.: +1-818-393-7799; fax: +1-818-393-5059.
E-mail address: nathan.bridges@jpl.nasa.gov (N.T. Bridges).
[1] Also at: Mars Surface Wind Tunnel, NASA Ames Research Center, MS 242-6 Moffett Field, CA, 94035.

0032-0633/$ - see front matter © 2003 Elsevier Ltd. All rights reserved.
doi:10.1016/j.pss.2003.08.026

arid regions. Of the three Mars landing sites, the Pathfinder site appears to show the most abundant ventifacts (Bridges et al., 1999) although some have been identified at the Viking sites (Binder et al., 1977; Mutch et al., 1977; Viking Lander Team, 1978; McCauley et al., 1979). Given the abundance of sand implied by widespread dunes and the effect of wind modification in the form of yardangs and other deflational features seen in orbital images (Breed et al., 1979; Lancaster and Greeley, 1990; Ward, 1979; Thomas and Weitz, 1989; Greeley et al., 1992; Malin and Edgett, 2001), it can be concluded that winds capable of moving sand have occurred. Most places on Mars consist of a mixture of exposed rocks and a finer component (Christensen, 1986; Golombek et al., 1999), such that rock abrasion should be a common geologic process, given sufficient time. Given the great age (generally > 1 Ga) of most mappable units (Tanaka et al., 1992) and the surficial geology (Golombek and Bridges, 2000), it seems likely that many Martian rocks have been abraded.

Numerous studies have been conducted on terrestrial ventifacts, although many are topical and in the older literature. Field studies (Blake, 1855; Blackwelder, 1929; Wentworth and Dickey, 1935; King, 1936; Maxson, 1940; Sharp, 1949; Higgins, 1956; Hickox, 1959; Lindsay, 1973; McCauley et al., 1979; Lancaster, 1984; Laity, 1992, 1994, 1995; Greeley et al., 2002), field plots combined with field studies (Sharp, 1964, 1980; Sharp and Saunders, 1978), analytical models (Anderson, 1986; White et al., 1976; and wind tunnel and other experimental studies (Kuenen, 1928, 1960; Schoewe, 1932; Whitney and Dietrich, 1973; Dietrich, 1977a, b; Whitney, 1978; Suzuki and Takahashi, 1981; Greeley et al., 1982) have identified heights and particle concentrations above the surface where maximum abrasion occurs, the types of ventifacts and their attributes, and relative susceptibilities to abrasion. All of these studies provide some important aspects of the complex processes of abrasion, the details of which will be discussed as warranted in this paper. Although general aeolian studies have been performed with boundary layer wind tunnels, no studies (to these authors' knowledge) have used such facilities to perform controlled experiments of abrasion and ventifact formation.

This paper reports on initial results from just such a study. We begin with a methodological overview of the wind tunnel experiments and field studies and follow with an analysis and interpretation of the resulting data and presentation of results. The implications for rock abrasion and ventifact formation on Earth and Mars are then discussed. We show that initial rock shape and texture play important roles in determining both rate and style of abrasion, with steep-sided, rough rocks eroding the fastest and intermediate-angled faces exhibiting the greatest shape change. We conclude that rocks tend to evolve toward an equilibrium shape whose form limits further abrasion. However many rocks on Mars and in terrestrial ventifact localities never reach this mature state, with erosion ceasing or slowing down due to exhaustion of the sand supply or to other factors, such as climatic shifts.

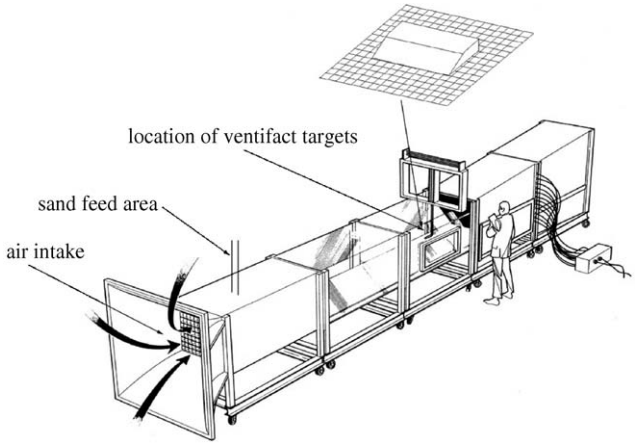

Fig. 1. Diagram of basic experimental setup for MARSWIT wind tunnel, Ames Research Center. Enlargement of ventifact target is shown at top. The size of the ventifact targets is seen in Figs. 2 and 4.

2. Methods

2.1. Wind tunnel experiments

To better understand the fundamental factors controlling rock abrasion and ventifact morphology, a series of experiments were conducted in which targets were abraded under controlled conditions. All experiments used the Mars Surface Wind Tunnel (MARSWIT) run by Arizona State University's Department of Geological Sciences and based at NASA's Ames Research Center, Moffett Field, CA (Fig. 1). An open-circuit boundary-layer wind tunnel, it has dimensions of 13 m (length) $\times$ 1.2 m (width) $\times$ 0.9 m (height) and is contained within a 4000 m^3 pressure chamber. Both terrestrial and Martian pressures are attainable. At Earth standard pressures ($\sim$ 1 bar), winds up to 11 m s^{-1} are achieved using a fan and motor system. Low (Martian) atmospheric pressures down to 3.5 mb are reached via a five-stage steam ejection plant, with winds up to 100 m s^{-1} generated by suction from a high-pressure air injection system at the exit end of the tunnel. Because 10 mb Earth atmosphere at standard temperature has a similar density and viscosity to 6 mb carbon dioxide at typical Martian temperatures, air is used instead of CO_2. Sand is fed through an adjustable, motorized hopper mounted on the top of the tunnel (90 cm above the floor), 1.3 m downwind from the flow straighteners and 4.0 m upwind from the targets. The hopper has a volume of $\sim$ 0.03 m^3, equal to about a standard bag (23 kg) of sand. Sand fluxes up to 0.6 kg min^{-1} are controlled by the size of the opening at the bottom of the hopper, with the speed of the motor capable of being accurately adjusted in real time. Instrumentation associated with the wind tunnel includes pressure sensors (pitot-static tubes and electronic pressure transducers), temperature sensors, an electrometer, humidity monitors,

and photographic equipment. Freestream wind velocity (v) is computed from the measured pressure differential (Δp) and density (ρ) using the standard formula:.

$$v = \sqrt{\frac{2\Delta p}{\rho}}. \quad (1)$$

The shapes of the abrasion targets are designed with flat sides at defined geometric angles to facilitate measuring volume and morphological changes as a function of geometry due to abrasion from windblown particles. The front face of each target is angled at either 15°, 30°, 45°, 60°, or 90° relative to the tunnel floor (angle A in Fig. 2c), with three different incidence angles (angle relative to wind as seen from above) per model (0°, 45°, and 60°) (Fig. 2b). The resolved angle (analogous to apparent dip) parallel to the wind stream and perpendicular to the floor is 11° (15° front face), 22° (30° front face), 35° (45° front face), and 51° (60° front face) for the 45° incidence angle faces and 8° (15° front face), 16° (30° front face), 27° (45° front face), and 41° (60° front face) for the 60° incidence angle faces. The width and length, along the dip slope, of the front faces of the targets are 8 and 5 cm, respectively, such that all faces have a surface area of 40 cm^2. The top faces of all the targets have a surface area of 92 cm^2, with the exact dimensions depending on the target shape. Abrasion target casts were made from an ABS-type plastic produced via numerically-controlled computer machining at Ames Research Center. Molds of the casts were then made out of a polymer at JPL from which "rocks" were made of a soft sandstone simulant. The simulant is composed of a mixture of either 225 μm- or 550 μm- mean diameter sand in a matrix of sheet rock (gypsum) paste and water. The material is strong enough to resist breaking, yet abrades when impacting sand either plucks matrix sand grains out of their sockets or preferentially erodes the softer interstitial sheet rock. This process causes the targets to lose mass and form ventifact-like features when subjected to impacting sand. As such, the targets serve as "abrasion maps," showing the areas and geometrical shapes most susceptible to abrasion under a range of controlled conditions. To test abrasion as a function of facet angle without regard to roughness factors present in the sandstone simulant targets, various foams cut into angled facets were also tested.

At the time of writing, the experimental matrix for the wind tunnel analysis under Earth conditions consisted of two materials (sandstone simulant and foam), five shapes defined by the angle of the front face relative to the wind as seen from the side (15°, 30°, 45°, 60°, and 90°), three runs of each target, and, in general, 3–4 repeats of this matrix, resulting in 99 experiments (54 for the sandstone simulant and 45 for the foam). The Earth experiments were run at freestream velocities of 11 m s^{-1}, typical saltation wind speeds in the terrestrial environment.

Six experiments at Mars pressure had been completed at the time of writing. These experiments are deemed necessary in order to assess the effect that lower pressure and

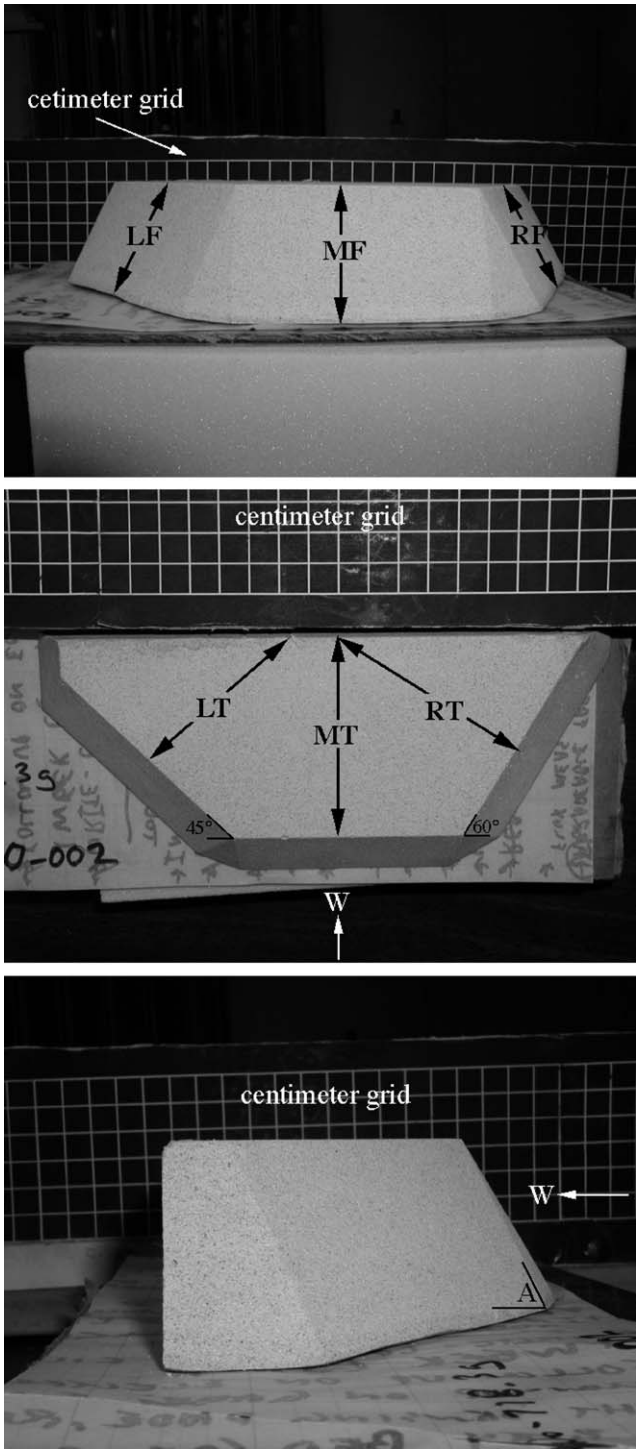

Fig. 2. Typical sandstone simulant target used in the wind tunnel and field experiments. Top is the front view, middle is the overhead view, and bottom is the side (left) view. Arrows labeled "W" in the lower two images show the downwind orientation of the targets when they are placed in the wind tunnel; the downwind direction is into the page for the top image. Grid with centimeter-size squares is in the background. This particular target is angled (A) 60° to the wind as seen from the side. Seen from above, the target presents three faces to the wind angled at 90°, 60°, and 45°. Dimensions measured during the experiments were left top length (LT), middle top length (MT), right top length (RT), left front height (LF), middle front height (MF) and right front height (RF).

higher wind speeds, conditions relevant to the aeolian regime on Mars (White et al., 1976), have on the saltation cloud and its ability to erode materials that are common in shape and composition to those used in the Earth pressure experiments. The Mars runs have so far consisted of 3 sandstone similunt shapes (15°, 45°, and 60°), each run two times. Wind speeds were at 58 m s^{-1} at the beginning of each experiment, with this value decreasing to 52 m s^{-1} as the line pressure dropped. These velocities are above that predicted to induce saltation in the Martian environment (Greeley and Iversen, 1985). Martian simulations, which are much more challenging to run because of the necessity of maintaining low and stable pressure, are ongoing.

All experiments used sand with a mean size of 550 μm (30 mesh). This is somewhat coarser than that found in terrestrial dunes, but is close to that thought to compose Martian dunes based on thermal inertia measurements (Edgett and Christensen, 1991). Using this size also increases the mass per sand grain, and thereby the momentum and kinetic energy, over that of smaller grains, such that the efficacy of abrasion is increased over that of smaller sized sand by the cube of the grain size (i.e., $KE = 0.5mv^2 = \rho\pi D^3 v^2/12$, where m is mass, v is velocity, ρ is density, and D is grain diameter (Greeley et al., 1982)). Sand flux from the hopper was 0.4 kg min^{-1} in all experiments. The total sand volume varied from 10 to 25 kg, such that the duration of any given run was 16 to 40 min. All targets were mounted 4 m downwind from the hopper (Fig. 1), a distance at which a sand cloud is sufficiently developed to approximate typical saltation conditions. No roughness elements were added to the floor of the wind tunnel because, although this is commonly done to simulate the wind speed profile necessary to induce saltation, the sand is these experiments was fed from a hopper such that inducing saltation was not necessary. Before and after each experimental run, the total sand expended, target weight, and target dimensions were recorded in order to gauge the effect of sand impact on mass loss and morphology (Table 1).

2.2. Field measurements

As a ground truth calibration, 15 sandstone simulant and foam targets of various shapes and resistances were placed at a ventifact site in the Little Cowhole Mountains, Mojave Desert, CA (USA) from May 17 to November 3, 2002 (Fig. 3 and Table 2). The targets varied in resistance and included soft gray foam, intermediate strength sandstone simulant, and resistant yellow foam. They were weighed and their dimensions measured before and after placement and a weather station at the site recorded average and maximum instantaneous wind speeds and directions every hour at a height of 2 m. The targets were mounted on heavy steel plates and positioned near ventifacts. The sandstone simulants were mounted to the plates with tacks and the foam targets were secured with strapping tape. The resulting data related mass loss and changes in morphological parameters to time, sand flux, type of target, and wind regime. The orientation of flutes on natural ventifacts at the locality, measured in earlier field work by co-author Laity and T. Boyle, were integrated with these results. As will be shown, these data were compared to the wind tunnel results to yield important insights into abrasion and ventifact formation on Earth and Mars.

This field site is east of Soda Lake and north of the Devil's Playground and Kelso Dunes. Both actively-forming and fossil ventifacts occur within the mountain range (Laity, 1995). Ventifacts along the topographic ridge are abraded on both their north- and south-facing sides, the two faces separated by a sharp keel. Rocks on the lower slopes show abrasion only on one face. Local micro-topography, such as notches or passes, acts to funnel wind flow, with ventifact grooves paralleling the notch axis (Laity, 1992). Sand is abundant. A small reversing dune occupies an area near the hill crest and a lee side dune extends to the south. Owing to the bi-directional nature of wind flow, sand is moved from one side of the site to the other, depending on season. Thus, in the largest sense, sand is always available for abrasion, although at any given time sand may be either overly abundant (burying a ventifact) or limited in supply (temporarily displaced elsewhere).

The weather station at the Little Cowhole Mountains is located on the crest of the hill, at the highest elevation in the study area (Fig. 3). It is situated so as to receive winds blowing from any direction at a height of 2 m. Significant saltation is observed when the main weather station registers a wind speed of 10 m s^{-1} at 2 m height, which is close to the 11 m s^{-1} wind speed used in the 1 bar wind tunnel tests.

3. Results

3.1. Wind tunnel experiments

3.1.1. Morphological changes

The observed, processes, rates, and nature of abrasion of the sandstone simulants provide important insights to ventifact formation. Without exception, abrasion of the sand grain matrix and interstitial cement composing the targets was heterogeneous, producing a texture that became qualitatively rougher over time (Fig. 4a). In many cases, subtle fluting on faces sub-parallel to the wind occurred during the final stages of the experiment (Fig. 4a, right). Reduced windflow in the lee of obstacles (large matrix grains or resistant nodules in the sandstone simulants and nails in the foam targets) resulted in differential erosion (Fig. 4b). The foam targets had mm-sized holes in their front faces prior to abrasion, which subsequently enlarged into pits about 5 mm in diameter (Fig. 4b). In two sandstone experiments, $\sim$ 1 cm diameter pits and flutes were gouged out of the targets prior to abrasion. These enlarged both in width and length with time (Fig. 4c). Visual evidence of slope retreat, in which the

Table 1
Wind tunnel experiments

Target type[a]	ΔMass (g)	Δ*LT*	Δ*MT*	Δ*RT*	Δ*LF*	Δ*MF*	Δ*RF*	Sand (kg)	Duration (min)	S_a[b] (g/kg)
Earth pressure										
15, sandstone (1.1)	0.4	3.2	−1.0	−2.9	−2.0	−2.0	−1.0	10.2	25.5	0.039
15, sandstone (1.2)	2.2	0.0	0.0	0.0	−1.0	0.0	0.0	13.5	32	0.16
15, sandstone (1.3)	3.9	−1.1	−2.0	0.0	0.0	2.0	0.0	12.6	36	0.31
15, sandstone (2.1)	1.9	−5.7	0.5	1.9	0.0	0.0	0.0	13.6	34	0.14
15, sandstone (2.2)	4.6	−1.1	−1.0	−1.0	0.0	0.0	0.0	12.4	32.5	0.37
15, sandstone (2.3)	5.8	0.0	−1.0	0.0	0.0	1.0	1.0	14.6	37	0.40
15, sandstone (3.1)	4.1	−0.2	−0.5	0.5	0.0	−1.4	−6.7	15.1	27	0.27
15, sandstone (3.2)	8.5	−1.1	−3.8	−0.2	−0.7	−0.2	0.1	14.7	27	0.58
15, sandstone (3.3)	6.8	0.0	0.0	0.0	0.0	0.0	0.0	12.7	30	0.54
30, sandstone (1.1)	8.3	0.0	0.0	0.0	0.0	0.0	0.0	12.7	30	0.65
30, sandstone (1.2)	9.1	−1.1	−1.0	0.0	0.0	0.0	0.0	12.7	33	0.72
30, sandstone (1.3)	5.3	−1.1	−2.0	0.0	0.0	1.0	0.0	12.5	32	0.42
30, sandstone (2.1)	3.7	0	−1.0	−1.0	0.0	0.0	0.0	13.6	34	0.27
30, sandstone (2.2)	6.6	−1.1	0.0	0.0	0.0	0.0	0.0	12.4	32.5	0.53
30, sandstone (2.3)	7.4	−2.1	−2.0	0.0	0.0	2.0	−1.0	14.6	37	0.51
30, sandstone (3.1)	2.8	0.0	−0.4	−0.3	0.7	0.9	0.2	15.1	37	0.19
30, sandstone (3.2)	10.9	−0.4	−2.9	0.4	0.6	1.2	−0.3	14.7	27	0.74
30, sandstone (3.3)	16.5	−0.9	−2.6	−1.4	0.4	0.3	1.7	14.8	37	1.11
30, sandstone (4.1)-p	8.7	1.5	1.7	1.2	−0.4	−1.3	−2.8	15.0	38	0.58
30, sandstone (4.2)-p	12.4	−0.9	−2.8	−1.3	−2.3	1.0	0.3	15.9	40	0.78
30, sandstone (4.3)-p	11.1	−1.2	−2.8	−0.4	−0.5	0.1	0.4	15.0	38	0.74
45, sandstone (1.1)	5.3	0.0	−0.5	1.9	0.0	0.0	0.0	12.7	30	0.42
45, sandstone (1.2)	7.9	0.0	−1.0	0.0	1.0	1.0	0.0	12.7	33	0.62
45, sandstone (1.3)	8.0	−1.1	−1.0	−1.0	0.0	0.0	0.0	12.5	32	0.64
45, sandstone (2.1)	9.0	0.4	−1.2	0.4	−1.5	−0.4	−1.0	15.1	36	0.60
45, sandstone (2.2)	16.9	−0.5	−1.3	−0.5	2.6	1.0	1.7	14.7	27	1.15
45, sandstone (2.3)	17.8	−1	−3.1	−0.1	1.0	1.8	0.6	14.8	37	1.20
45, sandstone (3.1)	9.7	−1.1	−2.9	−1.3	0.4	1.4	0.2	15.0	38	0.65
45, sandstone (3.2)	18.6	−0.6	−1.5	−1.4	0.8	0.9	1.2	15.9	40	1.17
45, sandstone (3.3)	18.1	−1.1	−1.9	−1.4	0.7	1.0	0.4	15.0	38	1.21
45, sandstone (4.1)	11.9	−0.5	−2.2	−0.9	1.4	2.1	−0.6	14.9	39	0.80
45, sandstone (4.2)	23.5	−2.4	−1.2	−0.6	−0.8	0.8	0.6	15.0	42	1.57
45, sandstone (4.3)	7.7	0.0	−2.5	−0.7	−0.9	0.2	0..2	15.6	42	0.49
60, sandstone (1.1)	11.3	−4.2	−3.0	−1.9	0.0	0.0	0.0	10.2	32	1.11
60, sandstone (1.2)	11.5	0.0	−1.0	0.0	0.0	0.0	0.0	12.6	36	0.91
60, sandstone (1.3)	9.8	0.0	−1.0	0.0	0.0	0.0	0.0	12.4	30	0.79
60, sandstone (2.1)	10.6	−1.1	0.0	0.0	0.0	0.0	0.0	12.7	30	0.83
60, sandstone (2.2)	13.2	−1.1	−2.0	−1.0	0.0	1.0	1.0	12.7	33	1.04
60, sandstone (2.3)	11.9	−1.1	−1.0	0.0	1.0	0.0	0.0	12.5	32	0.95
60, sandstone (3.1)	11.3	−2.1	−1.0	−1.9	0.0	0.0	0.0	13.6	34	0.83
60, sandstone (3.2)	11.1	−1.1	−1.0	0.0	0.0	0.0	0.0	12.4	32.5	0.90
60, sandstone (3.3)	11.8	−1.1	−2.0	−1.0	0.0	1.0	1.0	14.6	37	0.81
60, sandstone (4.1)-p	16.6	−0.7	−1.6	−0.7	−1.0	−2.9	−0.2	15.0	38	1.11
60, sandstone (4.2)-p	24.2	−3.3	−3.6	−1.9	0.0	2.3	0.5	15.9	40	1.52
60, sandstone (4.3)-p	11.1	−0.3	−1.9	−0.3	1.1	1.3	0.6	15.0	32	0.74
90, sandstone (1.1)	12.8	0.0	−0.2	0.0	0.0	0.0	0.0	10.2	32	1.25
90, sandstone (1.2)	14.7	−1.1	−2.0	−2.9	0.0	0.0	−1.0	12.6	36	1.17
90, sandstone (1.3)	14.9	−1.1	−2.0	−1.0	0.0	0.0	0.0	12.4	30	1.20
90, sandstone (2.1)	15	−0.8	−0.1	−1.2	−0.6	0.0	−0.2	14.9	39	1.01
90, sandstone (2.2)	8.2	−1	−2.4	−0.9	−0.1	−0.1	0.1	15.0	40	0.55
90, sandstone (2.3)	22.5	−0.8	−1.9	0.0	0.1	−0.3	0.0	15.6	42	1.44
90, sandstone (3.1)	16.7	−0.9	−3	−0.3	−0.4	−0.2	0.4	14.9	39	1.12
90, sandstone (3.2)	14.5	−1.4	−0.4	−1.3	0.1	−0.7	−0.7	15.0	40	0.97
90, sandstone (3.3)	13.6	−1.5	−2.7	−1.2	−0.5	0.6	0.5	15.6	42	0.87
Mars pressure										
60, sandstone (1.1)	32.0	−0.2	−0.4	−0.2	0.0	−0.1	0.1	14.3	38	2.24
60, sandstone (1.2)	28.3	−0.3	−0.3	0.0	0.0	0.0	0.1	11.7	29	2.42
45, sandstone (1.1)	49.9	−0.3	−0.7	−0.3	0.1	0.2	0.0	14.3	38	3.49
45, sandstone (1.2)	42.6	−0.5	−0.7	−0.4	0.0	0.3	0.2	11.7	29	3.64

Table 1 (*continued*)

Target type[a]	ΔMass (g)	Δ*LT*	Δ*MT*	Δ*RT*	Δ*LF*	Δ*MF*	Δ*RF*	Sand (kg)	Duration (min)	S_a[b] (g/kg)
15, sandstone (1.1)	15.7	−0.2	−0.3	−0.1	0.0	−0.3	−0.2	14.3	38	1.10
15, sandstone (1.2)	17.6	−0.1	−0.5	−0.2	−0.3	0.0	−0.2	11.7	29	1.50

Flux for all experiments was 0.4 kg min^{-1}, Earth and Mars pressure experiments were run at freestream velocities of 11 and 52-58 m s^{-1}, respectively. Δ*LT*, Δ*MT*, Δ*RT*, Δ*LF*, Δ*MF*, and Δ*RF* are dimensional changes in mm as defined in Fig. 1. "Sand" is the amount of sand (550 μm mean grain size) dropped from the hopper in the experiment.

[a]The first number (e.g., 15, 30, etc.) refers to the incident angle of the front face of the target. "Sandstone" is the sandstone simulant (not sandstone rock) discussed in the text. The first number in parenthesis (e.g., the "2" in 2.1) is the abrasion target ID. The second number (e.g., the "1" in "2.1") is the run number for a given target. "pp." indicates targets that had pits gauged into their front faces prior to the first abrasion run.

[b]The effective susceptibility to abrasion, computed as the mass loss from the target divided by the amount of sand used in the experiment.

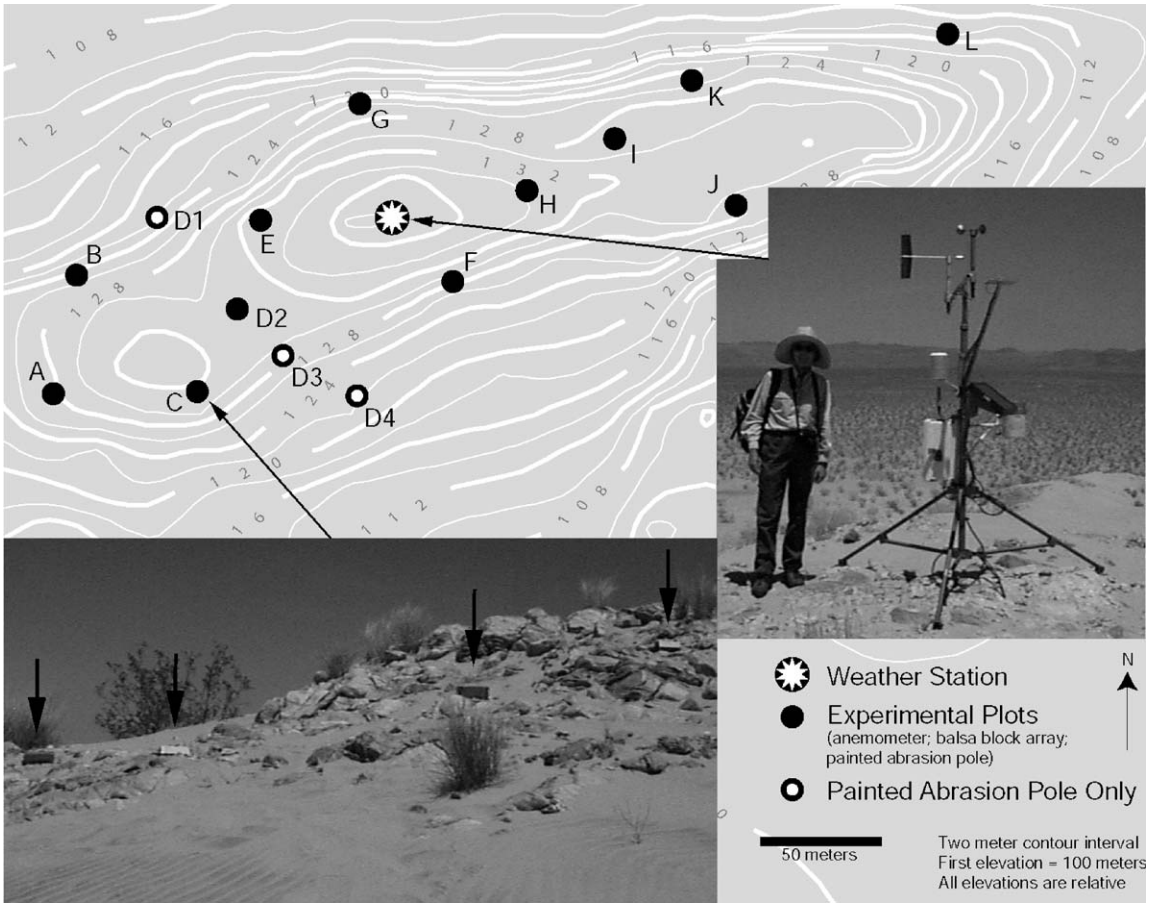

Fig. 3. Map and pictures of ventifact study area in the Little Cowhole Mountains in California's Mojave Desert (USA). Map shows stations used for this work and in the study of Boyle (2001). Stations C, D2, and H were used for our experiments. Pictures show targets at Station C prior to abrasion (left) and the weather station located at the hill crest (right).

upper part of the target eroded back farther than the lower part, forming a basal sill, also occurred (Fig. 4a and d). All of these characteristics are observed in natural ventifacts (Laity, 1994).

3.1.2. Mass loss

Some of the most important morphological changes are tracked and quantified by plotting mass and dimensional changes and their associations with time. Plotting mass loss from the sandstone simulant targets vs. sand mass from the hopper shows that mass loss is proportional to front facet angle (*A* in Fig. 2), with higher angled surfaces exhibiting a greater amount of abrasion per amount of sand (Fig. 5a), which effectively translates into abrasion rate because the sand flux was constant among all the experiments. The greatest mass loss was exhibited by the pre-pitted samples. In 64% of the sandstone experiments, the amount of mass loss divided by the amount of sand used was greater in a

Table 2
Field measurements of analog targets

Target type	Station bearing of front face		ΔTarget mass (g)		Δ*MT* (mm)	Final Angle (°)	Δ Angle (°)
45, sandstone	D2	S30°E	563.9[a]	(78%)	NA	34	11
90, sandstone	C	S33°E	382.9	(62%)	66.0	50	40
45, gray foam	H	S23°E	42.0[b]	(58%)	42.0	40	5
60, gray foam	D2	S36°E	−1.4	(−6%)	33.3	47	13
90, gray foam	D2	S67°E	−3.0	(−17%)	14.5	65	25
45, yellow foam	D2	S40°E	4.0	(6%)	5.8	45	0
60, yellow foam	C	S74°E	−2.7	(−3%)	1.7	60	0

[a]Target broke into two pieces between May and November, 2002.
[b]In November, 2002, the target was weighed under high wind conditions, so the mass change may be suspect.

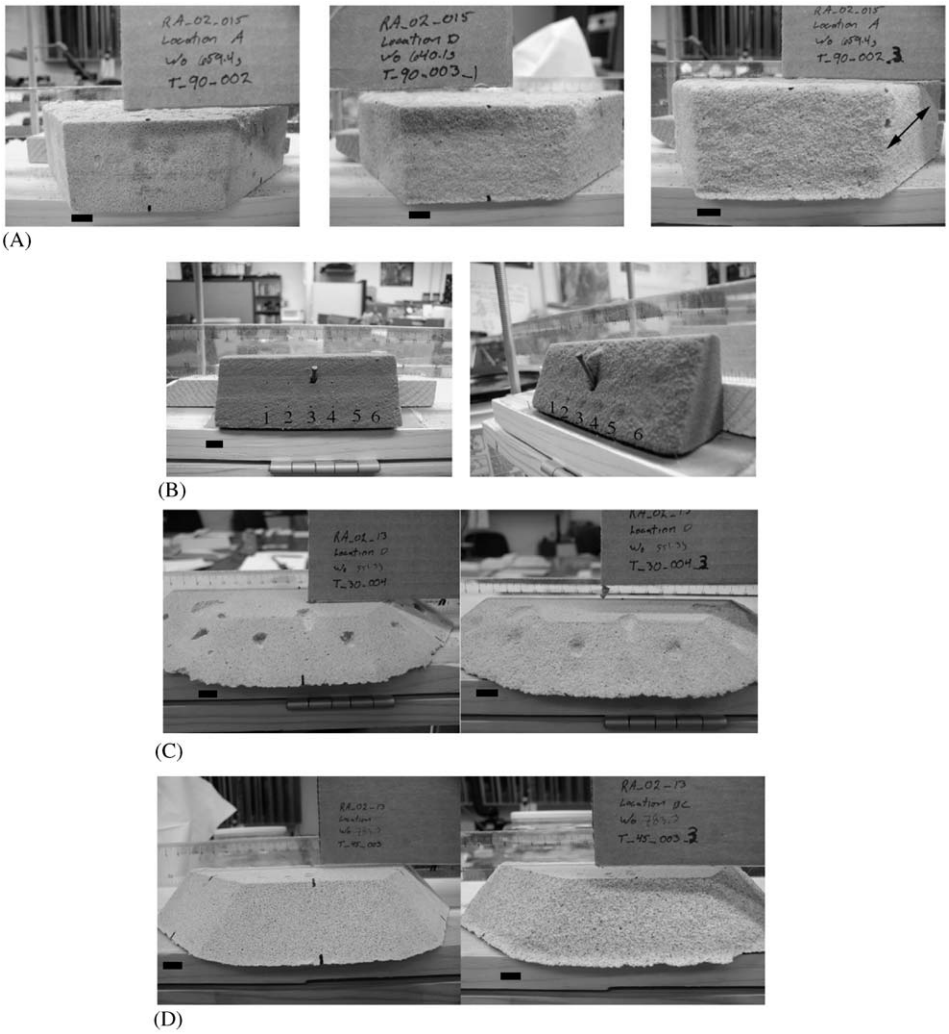

Fig. 4. Morphological and textural evolution of analog targets in the wind tunnel after being subjected to abrasion at Earth pressure. Black bar in images represents a distance of 1 cm for the middle, front part of each respective target. (A) Sandstone simulant prior to abrasion (left), after one abrasion run (middle), and after three abrasion runs (right). Note the increase in roughness, subtle fluting on right edge, and the formation of a basal sill. Front face has an angle of attack to the wind of 90°. (B) Enlargement of mm-sized holes, labeled 1 through 6, in gray foam targets (left is before abrasion, right is after three abrasion runs). Also note the slope retreat, evident by the preserved foam behind the nail. The front face has an angle of attack to the wind of 60°. (C) Enlargement of pre-existing pits in sandstone simulant target (left is before abrasion, right is after three abrasion runs). The front face has an angle of attack to the wind of 30°. (D) Development of basal sill after three abrasion runs of a sandstone simulant target. The front face has an angle of attack to the wind of 45°.

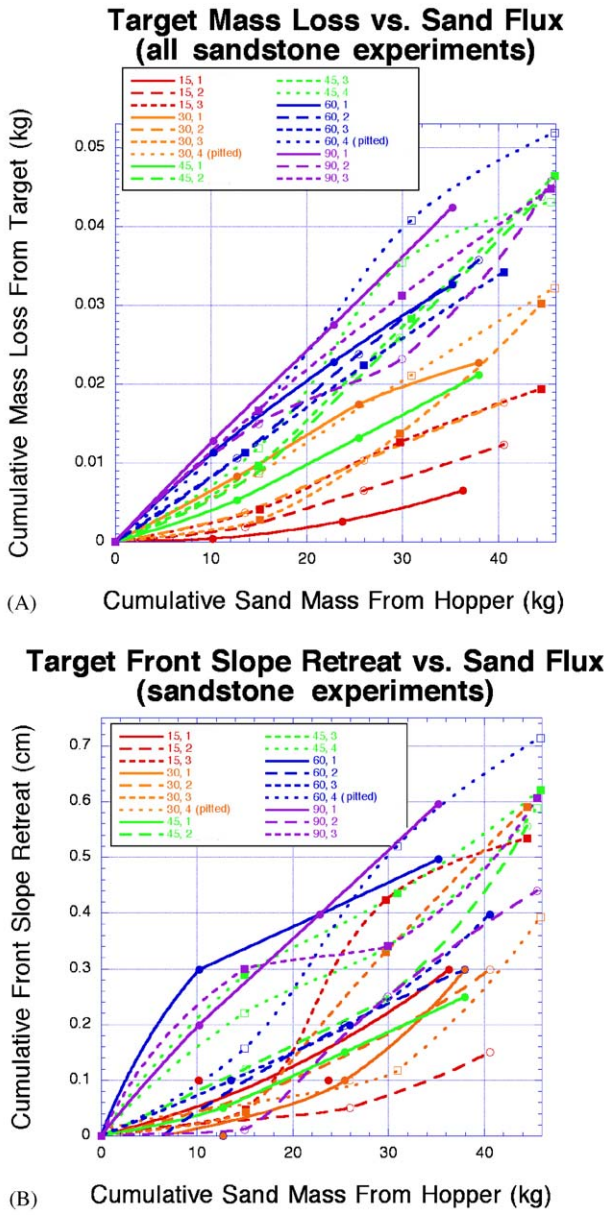

Fig. 5. Mass and morphometric changes of the sandstone simulant targets at Earth pressure. In the legend in the upper left of both plots, the first number is the angle of the front face of the target relative to horizontal ($\sim$ windstream) as seen from the side. The second number is the target ID (e.g., the results of three 15° targets and four 30° targets [one pitted] are plotted). The data points represent results following a run for a given target. Curves are interpolations between the data points for a given target. (A) Cumulative mass loss as a function of sand mass used in the experiment. (B) Slope retreat (ΔMT in Fig. 2 and Table 1) of the middle face as a function of sand mass used.

given run compared to the previous run (Table 1). Interpretations of these results are discussed in the next section.

3.1.3. *Morphometric changes*

The retreat of the top face (ΔMT, the change in length of the top face, measured from the mid-center in a perpendicular direction to the back (Fig. 2)) relative to cumulative hopper sand (Fig. 5b) is somewhat correlated to facet angle, but not as clearly as mass loss is. In almost all cases, the retreat of the front face (MT, oriented 90° in plan view to the wind) was greater than that of the left face (LT, oriented 45°) which in turn is greater than the right face (RT, oriented 60°) (Table 1). The change in top front center depth vs. front center height for sandstone simulant targets (ΔMF and ΔMT, respectively, in Fig. 1 and Table 1) is shown in Fig. 6. The error of measurement is on the order of a millimeter, so that these graphs give but an approximate view of erosional behavior. Observations show little rounding of the front face-to-top face edge, such that overall slope retreat is considered a greater factor (e.g., note lack of significant rounding of targets in final stages of abrasion in Fig. 4). Because only dimensions from the target edges were measured, non-planar aspects of the abrasion could not be quantified. Therefore, the interpretation of planes eroding back, or changing slope, averages what may be more complex and detailed shape changes across the whole surface of the target. The plots show three zones. The upward sloping line is where $\Delta MT = \Delta MF$ cos(angle), a condition in which all of the change in front face length is fully accommodated by a change in top face length. No points should plot to the left of this line and, indeed, only one is found, for the 30° target data, which can be explained by measurement error. An increase in MF ($+\Delta MF$) must be accommodated by a decrease in slope; e.g., a full accommodation would have the hinge line at the front base of target. Similarly, a decrease in MF must result in a steepening slope, with the hinge line being at the front top of the target (except for the case of targets with a 90° front face, the slope of which can only decrease). Where ΔMF is 0, indicated by the horizontal black line, the target maintains its shape via even retreat of the front face. In this case there is no hinge line and, although the target erodes, there is no morphometric change. The plots show considerable scatter, but some interesting relationships can be retrieved. Targets with front faces of 30°, 45°, and 60° exhibit shallowing of their front faces. The pre-pitted 30° and 60° targets initially steepen, then shallow, but the limited number of these experiments makes it difficult to confidently interpret these results. Within the measurement error, the 90° targets maintain their shape. The 15° target data are the most scattered of any of the forms, but, on average, also exhibit a tendency to maintain their shape. The terrestrial results are non-linear with angle and may seem counterintuitive, but, as well be shown, can be easily explained. The limited number of Martian tests show virtually no change in target shape or dimensions, but more experiments are needed to confidently interpret the results.

The integrated observations are: (1) the targets whose shape is most perpendicular to the wind abrade the most and at the fastest rate, and (2) from what can be determined within experimental error, there is a tendency for shallowing of target front faces of intermediate slope angle (30–60°), with very steep (90°) and very shallow (15°) targets more or less maintaining their shape.

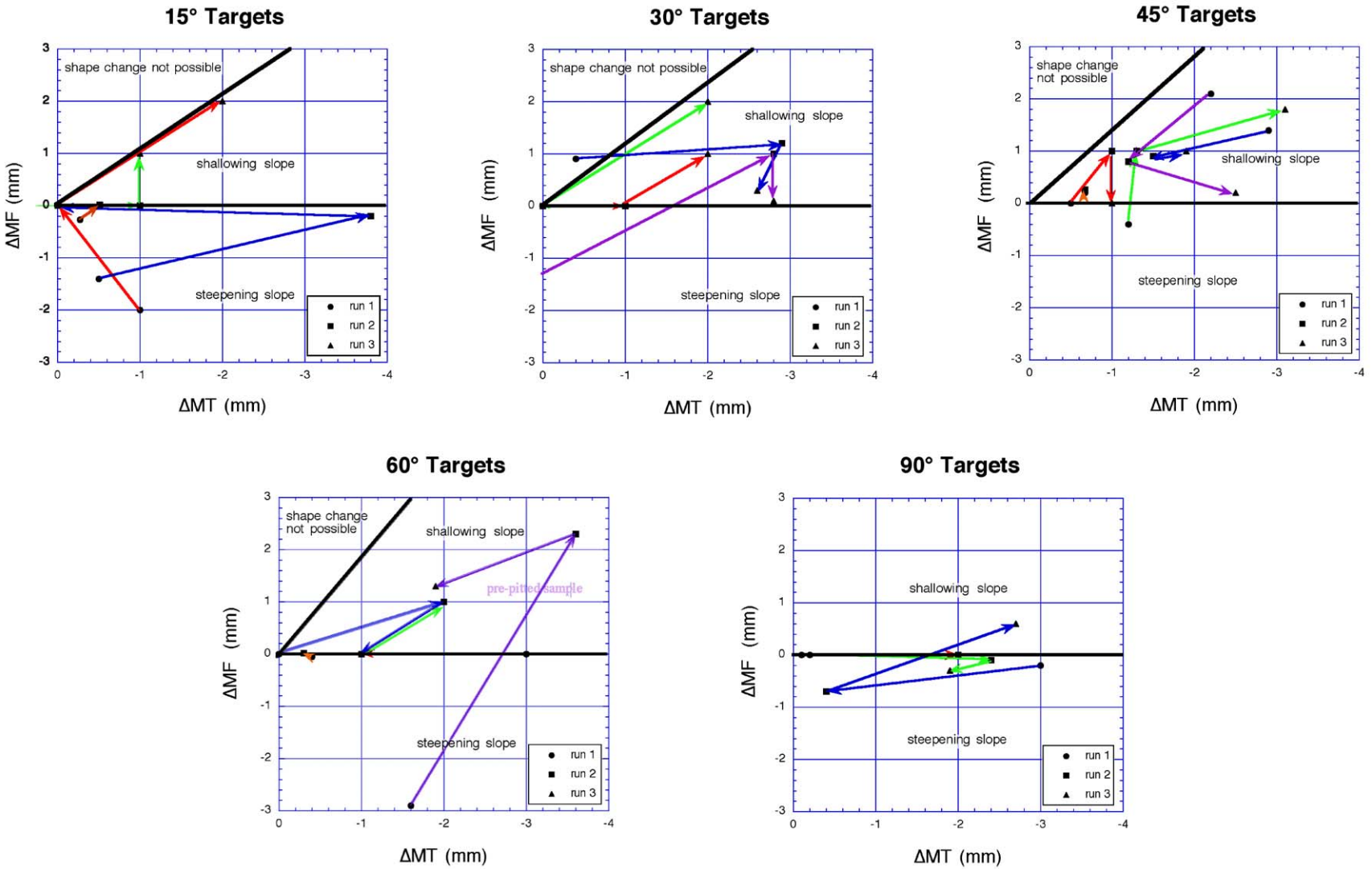

Fig. 6. Morphometric evolution of top (ΔMT) and front face (ΔMF) dimensions for the sandstone simulant targets at 1 bar pressure. Note that these graphs show the changes (Δ) in dimensions, not the dimensions themselves. Arrows show progression direction between experimental runs, with the points representing the measurements at the conclusion of the given runs (e.g., point xx, 1 is the dimensional change after the first run; xx, 2 is the change after run 2 relative to run 1; xx, 3 is the change after run 3 relative to run 2). Dark lines define regions where, theoretically, slopes should be steepening or shallowing.

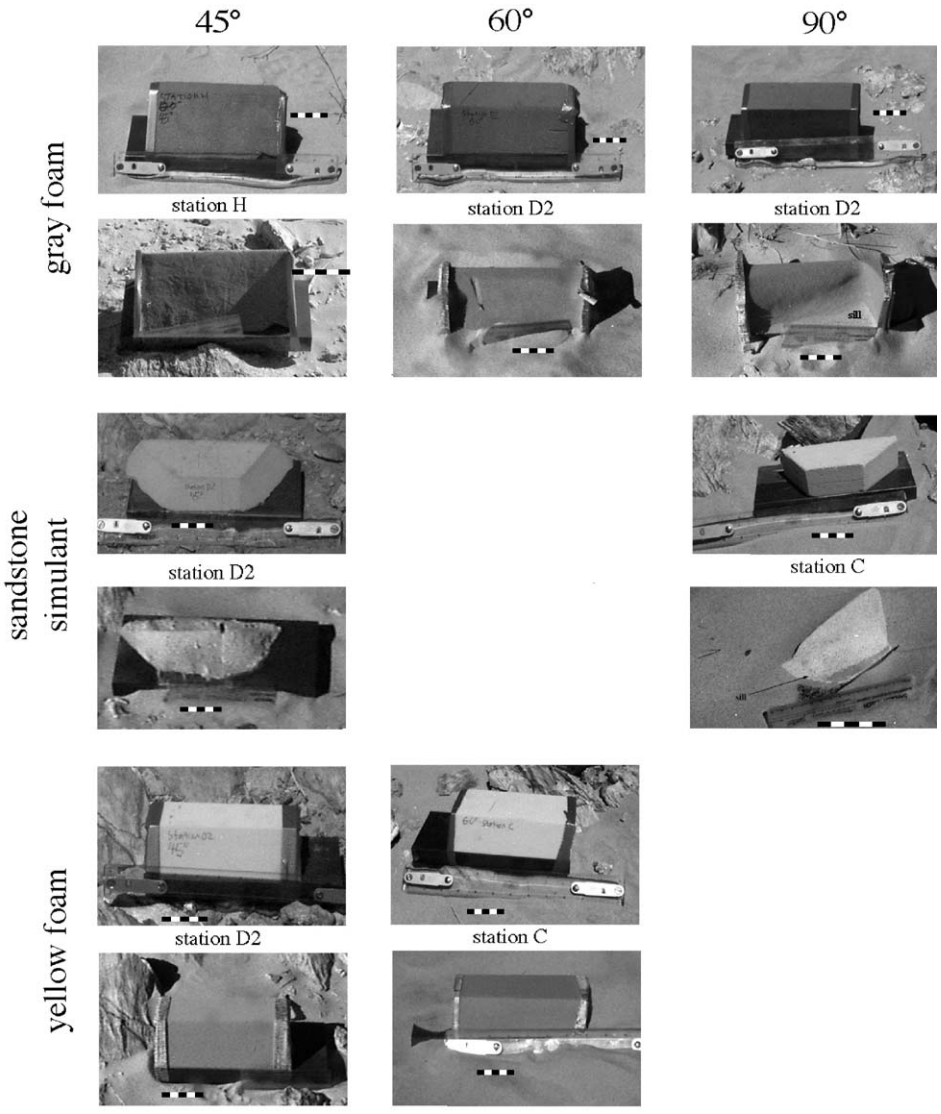

Fig. 7. Morphologic evolution of analog targets at the Mojave site. Top row for each target is prior to abrasion, in May 2002. Bottom rows are after abrasion in November, 2002. Each black and white bar represents a distance of 1 cm for the middle, front part of each respective target.

3.2. Field experiments

3.2.1. Morphological changes

Upon returning to the field site after six months in November, 2002, 8 of the 15 original targets could not be examined because they were deeply buried by sand, attesting to the dynamic nature of the aeolian environment. The remaining 7 targets, of varied strengths and shapes, allowed assessment of natural wind erosion. Not surprisingly, erosion was most significant on the soft gray foam targets and least on the resistant yellow foam (Fig. 7, Table 2). Maximum erosion on all targets occurred on the south side, as anticipated after a summer season (see below). Minor abrasion also occurred on the north faces of targets at stations D2 and H, located on a topographic saddle, where winds have a bi-directional component. Subdued, small scale flutes and grooves (lineations), oriented nearly perpendicular to target strike (i.e., close to N–S), developed on the sandstone targets and the 45° and 60° gray foam targets. The 90° gray foam and sandstone targets developed a thin sill of non-eroded material at their base.

3.2.2. Mass loss and morphometric change

Interpretation of the mass loss and morphometric data were compromised by nature's variability over 6 month's time in the desert, a situation not encountered in the controlled wind tunnel experiments. Some targets were partially or completely buried by migrating sand and it is uncertain how many burial and exhumation episodes may have occurred over the half year span. Slope retreat was difficult to gauge on some sandstone targets because they had eroded to their back edges. It was more obvious on the foam targets,

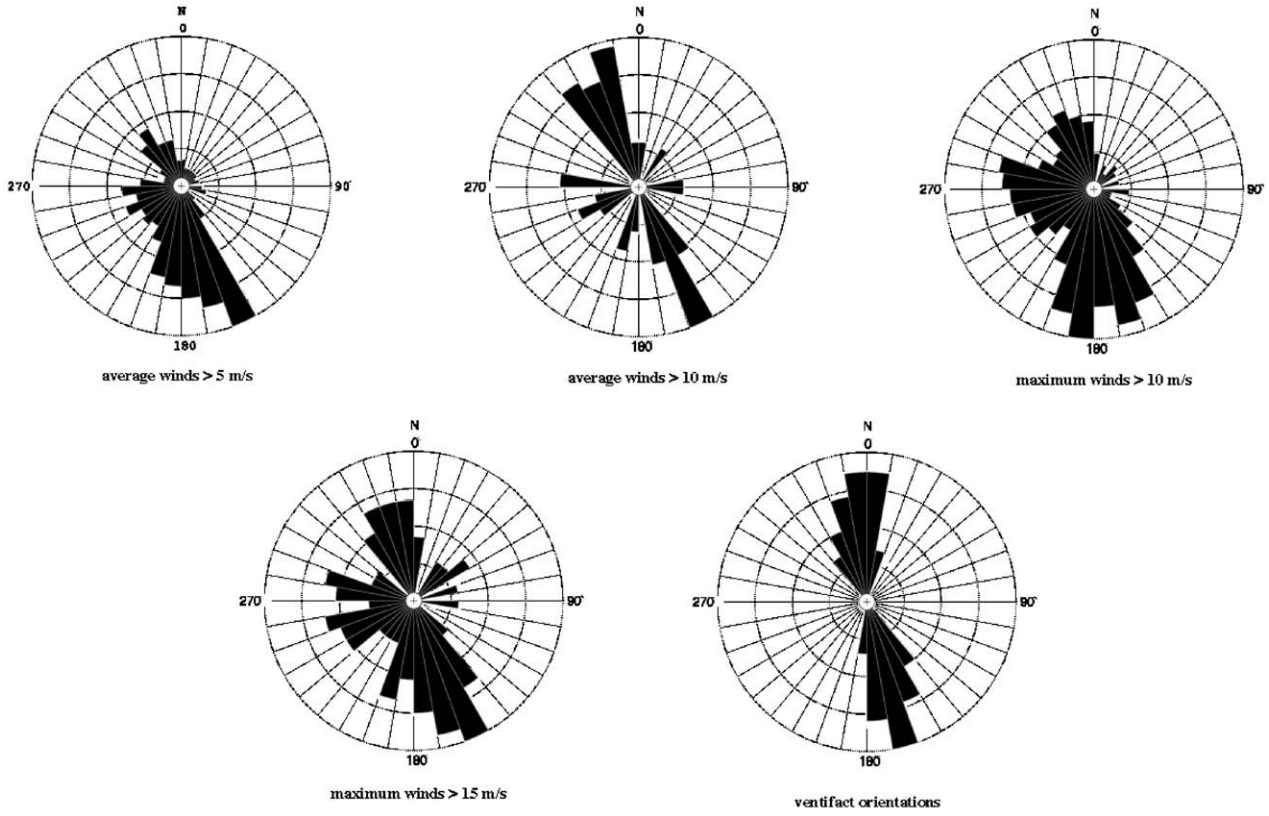

Fig. 8. Equal area rose diagram showing winds during May to November, 2002 and local ventifact orientations at the Mojave field site. Forty ventifact measurements were made.

including the hard yellow ones, because the original faces and edges were preserved behind the strapping tape. The distance from the strapping tape to the eroded target face showed retreat of several centimeters for the gray foams and a few millimeters for the yellow foams. Despite the complexities of data interpretation, several consistent observations emerge: (1) the softest targets eroded the most, (2) the sandstone and gray foam targets with greatest original face angle exhibited the greatest angle change, with 90° targets changing their angle about 4× as much as 45° targets. Targets seemed to evolve toward angle of ~ 30° given enough time, (3) the sandstone targets became rougher, and (4) the 90° targets formed basal sills.

3.2.3. Comparison to wind and ventifact data

Analyzing data from the weather station for the study period of May–November 2002 shows typical summer weather patterns. The automated weather station made 4079 measurements of hourly average and maximum wind speeds and their directions during this time. Average and maximum wind speeds > 10 m s^{-1}, a value close to that needed to induce threshold (the exact value depends on the surface roughness, which in this setting is mainly controlled by the size, shape, and abundance of rocks), made up 1.3% and 14.2%, respectively, of the measurements. A plot of winds greater than 5 m s^{-1} exhibits a predominance of southeasterly flow, characteristic of the summer season (Fig. 8). By contrast, the wind rose plot of winds greater than 10 m s^{-1} illustrates a strong bi-directional distribution (NNW–SSE). These observations mirror those compiled over 1993–1998 (Boyle, 2001). The orientation of flutes on the ventifacts indicates that higher velocity winds are better correlated to abrasion than the integrated energy from lower velocity flow over time

4. Discussion

Previous studies have addressed the importance of rock shape, texture, hardness (or resistance to abrasion), wind regime, and local environment on rock abrasion and ventifact formation. In this section, we integrate the laboratory and field investigations, incorporating these previous and other ongoing studies, to provide quantitative assessments of many of these factors as well as an improved understanding of their inter-relationships and relative importance on Earth and Mars. Many of these factors are complexly linked and exert positive or negative feedback effects on each other. For simplicity, we first address each factor individually before discussing a coherent model of rock abrasion and ventifact formation.

4.1. Initial rock shape

Initial rock shape determines the rate of mass loss, the rate and style of morphologic change, and the rate and style of textural change. Steep faces erode faster than more shallow faces. This is in agreement with other field studies using gypsum and brick blocks that showed front-to-side and front-to-top cutting ratios of 20:1 and 45:1, respectively (Sharp, 1980). Previous experiments in which the susceptibility to abrasion (S_a) was measured using a rotary sand slinger (Greeley et al., 1982) found that crystalline igneous rocks (granite, rhyolite, and basalt) had S_a values proportional to impact angle in the range of 30° to 90°, in agreement with our experiments. However, the Greeley et al. results also show an increase in susceptibility below 30°, which we have not observed. They attribute this to an effective cutting and gouging mechanism by shallow impacting sand grains. One explanation for the discrepancy between our and the Greeley et al. results is that the wind tunnel experiments better simulate the likely grain motions within a sand cloud and their interaction with a target of a given angle. Saltating sand grains have trajectory angle ranges of approximately ±10–20° (White and Shulz, 1977), with the negative values referring to the angle as the grain leaves the surface and the positive values the angle as the grain descends. Particles on the ascending part of the saltation path, accounting for 50% of the sand cloud, will either not hit or at most interact tangentially with any slopes in the 15–20° range. It is therefore likely that, when sand cloud motions are considered and our experimental results folded in, that steeper faces erode more rapidly than shallow faces as they are impacted by both ascending and descending grains.

We also observe that intermediate angled faces tend to exhibit the greatest angle change (but not the greatest mass loss). We hypothesize that this is due to preferential differential erosion as a function of height on intermediate angled faces compared to steeper and shallower faces. In nature, the combination of grain size, flux, and velocity vary with height, such that there is an optimum distance above the surface, generally at 10–40 cm, at which the greatest abrasion, or kinetic energy transfer, occurs, with the exact value depending on roughness and other factors of the field setting (Sharp, 1964, 1980; Anderson, 1986). As observed by Greeley et al. (1982), some rock abrasion occurs by cutting and gouging of material at shallow impact angles. In a saltation cloud, the upper part of the cloud contains the flattest trajectories and highest average particle velocities. A greater fraction of grains impact the upper part of a rock surface than the lower parts, where intersecting trajectories are steeper. If the rock front face is oriented at an intermediate angle, greater kinetic energy transfer, cutting, and gouging occurs on the upper face, resulting in greater retreat than the lower face and a shallowing of the overall face angle. Very steep faces, such as the 90° targets in the abrasion experiments, abrade more or less evenly because the impact angles are all in the 70–90° range, regardless of height, and the high KE of grains on the upper face is balanced by the lower face receiving impacts from both ascending and descending grains (target faces oriented less than 90° are only impacted by descending grains). Grain trajectories intersecting a shallow-angled rock are low enough such that differential erosion between the top and bottom faces is insignificant. In other words, the intermediate angled faces cause the impacting particles to have greater erosion on the upper vs. the lower part of the face, resulting in a flattening of slope angle with time.

The process just described also influences the texture and textural change with time. In experimental conditions, steep faces to the wind become pitted. By contrast, oblique and shallow faces developed shallow grooves (Fig. 4a). Similar relationships to slope angle are observed in nature, with steep angled faces generally being heavily pitted over their whole exposed area and intermediate angled faces exhibiting the greatest concentration of flutes and grooves on their upper parts (Sharp, 1949; Laity, 1994, 1995).

4.2. Rock texture

The wind tunnel studies provide two forms of evidence that rock texture influences the style and rate of abrasion. First, as the targets are abraded, they become rougher and, more often than not ($\frac{2}{3}$ of cases in our experiments), the rate of abrasion (mass loss) increases concomitantly. In our experiments, the reason that mass loss increased with time for $\frac{2}{3}$ of the cases versus all of the time or half the time is not known, but we hypothesis that the process is somewhat random, with a bias toward an increase in roughness and mass loss with time. Second, targets with pre-existing pits lose more mass than non-pitted samples. The ability of pits to serve as nucleation sites has been proposed by previous workers (Whitney, 1978; Greeley and Iversen, 1985), but never seen experimentally. Precisely how puts increase the mass loss from rocks is not known, but may involve greater erosion from vortical recirculation of particles (Whitney, 1978) or sand grain rebounds within pits (R. Sullivan, personal communication, 2003).

4.3. Rock hardness

It is not surprising that hard rocks are less susceptible to abrasion than soft rocks. Our work does not add to this obvious fact (although, perhaps not so obvious is the observation of Lancaster (1984) that abrasion features are best developed on fine-grained rocks of intermediate hardness). However, for a given hardness (which sometimes can be related to rock type), we show that texture and shape are driving factors in determining the rate and form of abrasion.

4.4. Wind regime

Not surprisingly, rocks, and our wind tunnel and field targets, abrade most heavily on windward sides. This argues against the hypothesis of Whitney and Dietrich (1973) and Whitney (1978) that dust within vortices on the downwind sides of rocks is a significant abrasion process. The orientation of ventifact features, such as elongate pits, flutes, and grooves, result from high velocity winds (Fig. 8) and is in agreement with other field investigations (Lancaster, 1984). This is due to two factors: (1) The kinetic energy of saltating particles varies with the square of the velocity, such that mass losses are non-linearly correlated with impact velocity (compare the mass loss of targets under the differing terrestrial and Martian wind speeds). For example, theoretical studies indicate that the kinetic energy flux scales with the fifth power of the wind shear velocity (Anderson, 1986). (2) At speeds below 5–10 m s^{-1} (with the exact value depending on the surface roughness, which determines saltation friction speed (Raupach et al., 1993)), particle saltation is not initiated, so there is no sand to induce rock abrasion. Therefore, determining ancient climatic regimes on Earth and Mars based on ventifact flute and groove orientations reveals little about average wind direction unless the average velocities are great enough to induce saltation. Generally this is not the case, so that flutes correlate to the highest winds in a given climatic regime.

4.5. Local surface environment

The final factor is local environment, itself composed of a complex set of inter-related parameters that cannot be easily simulated in the wind tunnel. Field experience shows that the mobile surface layer of sand is as much an abrader of rocks as it is a shield for further abrasion. Winds capable of saltating sand onto near-surface rocks (in the 10s of centimeters height range) in energy-transferring collisions also act to move it en masse to cover these rocks. Near surface rocks are commonly completely buried by sand within an hour. This process not only shields the buried parts of rocks, but also alters the local aerodynamic roughness and the height of exposed rocks above the surface, thereby changing the abrasion as a function of position on the rock. Local topography acts to funnel and alter wind directions, thereby influencing flute and groove orientations. This is exemplified by our field studies, which show abrasion on both sides of targets where they are located on a topographic saddle. Finally, the positions of rocks relative to one another, and their shape, and height, influence how and where sand grains saltate. For example, very rough surfaces containing many rocks cause saltating grains to bounce high into the air, thereby increasing the grain velocity and kinetic energy. At the same time, a high rock abundance limits the sand supply, resulting in less abrasion. The combined effect of these and other factors is difficult to model.

4.6. Summary of integrated effects and implications for understanding rock erosion on Mars

Prior to any wind modification, the shape and texture of a rock are obviously the result of primary and modification processes. Rocks that are steep-sided and rough are more apt to lose mass from abrasion than flatter and smoother rocks. Intermediate sloped rocks with rough surfaces will tend to become fluted and grooved, whereas steep-sided rocks should become more pitted, with the size of pre-existing pits enlarging with time. Slope retreat and basal sill formation, whereby the upper part of a target or rock erodes more rapidly than the base (Laity, 1994) are common. All of these features are observed on terrestrial and Martian ventifacts (Fig. 9). Erosion, grooving, and slope retreat occur on faces oriented in the direction of high speed winds rather than average winds. It is expected that over time rocks with initially inclined windward facets will evolve to slopes of approximately 30° or so, with shallower and steeper rocks more or less maintaining their shapes. Many rocks will never reach this state because abrasion ceases due to exhaustion of the sand supply, rock burial, or changing climatic conditions.

The field and laboratory studies give insight into not only the factors controlling rock abrasion and ventifact formation on Earth, but also on Mars. Although our wind tunnel studies are still ongoing, combining the limited low pressure runs already completed with the terrestrial results gives insight into rock abrasion processes on Mars. Fundamentally, there should be little difference between the factors controlling rock abrasion on the two planets. The main differences in the aeolian environment on Mars compared to Earth is the lower atmospheric pressure and gravity, which together result in higher saltation friction speeds, longer trajectory paths, and flatter trajectory angles. This first factor results in more rapid abrasion on Mars compared to Earth, as verified in our experiments (Table 1) and earlier work by Greeley et al. (1982). The second factor probably makes little difference. The third factor results in a rock face on Mars being subjected to a greater fraction of low angle impacts. This should cause greater differences between the abrasion of steep faces versus shallow faces compared to the difference on Earth. The compositional differences in sand on Earth and Mars may also be important. Most abrading sand on Earth is made of quartz, the hardest common rock forming mineral. On Mars the composition of sand is not known, but the probable lack of large scale granitic source rocks suggests that it may be composed predominantly of softer mafic minerals (Smalley and Krinsley, 1979). Another major distinction between Earth and Mars is the weather and climate. Desert regions on Earth commonly have many 10s of saltation events per year. On Mars today, freestream wind speeds sufficient to induce saltation, probably about 30 m s^{-1}, are rarely reached (Ryan and Henry, 1979; Greeley et al., 1982; Schofield et al., 1997) consistent with the generally old age inferred for surface modification (Golombek and Bridges, 2000) and the lack of large scale

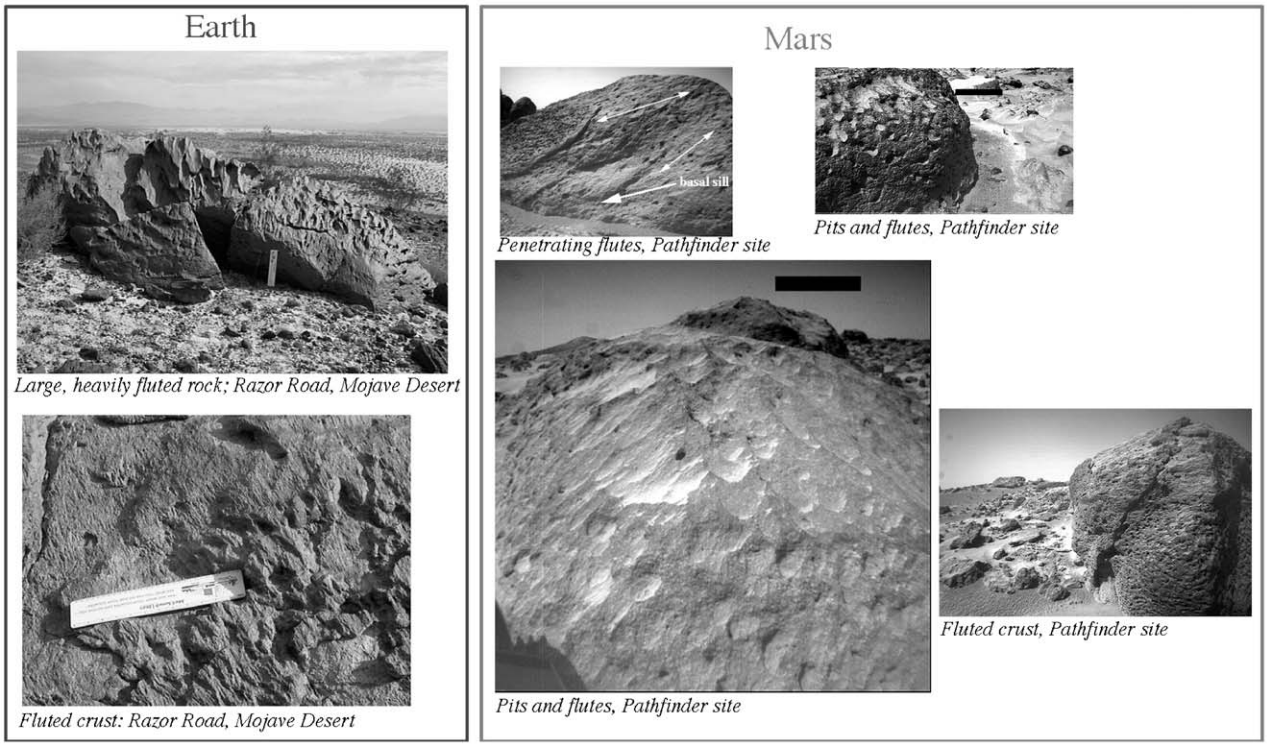

Fig. 9. Example of ventifacts on Earth and Mars. Note prevalence of pits on steep faces and basal sill in upper left Mars example.

dune motion seen in high resolution images (Edgett and Malin, 2000; Zimbelman, 2000; Malin and Edgett, 2001). This suggests that the ventifacts seen on Mars either formed slowly over time in widely separated abrasion episodes or date from a previous era when winds were stronger and abrasion more common. Future wind tunnel experiments at Martian pressures should explore these problems in greater detail and hopefully further address some of these issues.

Acknowledgements

Detailed reviews by N. Lancaster and R. Sullivan significantly improved the manuscript. We are grateful to T. Boyle for letting us use his wind data at the Mojave site and his map shown in Fig. 3. G. Zavala-Diaz and G.E. Krammer assisted in some of the wind tunnel work. C. Meyer performed sand flux calibrations in the wind tunnel. All experimental work was performed at the Mars Surface Wind Tunnel (MARSWIT) run by Arizona State University's Department of Geological Sciences and based at NASA's Ames Research Center, Moffett Field, CA. This investigation was funded under a grant from NASA's Planetary Geology and Geophysics Research Program.

References

Anderson, R.S., 1986. Erosion profiles due to particles entrained by the wind: application of an eolian sediment-transport model. Geol. Soc. Amer. Bull. 97, 1270–1278.

Binder, A.B., Arvidson, R.E., Guinness, E.A., Jones, K.L., Morris, E.C., Mutch, T.A., Pieri, D.C., Sagan, C., 1977. The geology of the Viking Lander 1 site. J. Geophys. Res. 82, 4439–4451.

Blackwelder, E., 1929. Sandblast action in relation to the glaciers of the Sierra Nevada. J. Geol. 37, 356–360.

Blake, W.P., 1855. On the grooving and polishing of hard rocks and minerals by dry sand. Am. J. Sci. 20, 178–181.

Boyle, T.K., 2001. Ventifact formation, Little Cowhole Mountains, East-Central Mojave Desert. Master's Thesis, Department of Geography, California State University, Northridge.

Breed, C.S., Grolier, M.J., McCauley, J.F., 1979. Morphology and distribution of common "sand" dunes on Mars: comparison with the Earth. J. Geophys. Res. 84, 8183–8204.

Bridges, N.T., Greeley, R., Haldemann, A.F.C., Herkenhoff, K.E., Kraft, M., Parker, T.J., Ward, A.W., 1999. Ventifacts at the Pathfinder landing site. J. Geophys. Res. 104, 8595–8615.

Christensen, P.R., 1986. The spatial distribution of rocks on Mars. Icarus 68, 217–238.

Dietrich, R.V., 1977a. Impact abrasion of harder by softer materials. J. Geol. 95, 242–246.

Dietrich, R.V., 1977b. Wind erosion by snow. J. Glaciol. 18, 148–149.

Edgett, K.E., Christensen, P.R., 1991. The particle size of Martian aeolian dunes. J. Geophys. Res. 96, 22,765–22,776.

Edgett, K.S., Malin, M.C., 2000. New views of Mars eolian activity, materials, and surface properties: three vignettes from the Mars Global Surveyor Mars Orbiter Camera. J. Geophys. Res. 105, 1623–1650. 2000.

Golombek, M.P., Bridges, N.T., 2000. Erosion rates on Mars and implications for climate change: constraints from the Pathfinder landing site. J. Geophys. Res. 105, 1841–1853.

Golombek, M.P., Moore, H.J., Haldemann, A.F.C., Parker, T.J., Schofield, J.T., 1999. Assessment of Mars Pathfinder landing site predictions. J. Geophys. Res. 104, 8585–8594.

Greeley, R., Iversen, J.D., 1985. Wind as a Geological Process on Earth, Mars, Venus, and Titan. Cambridge University Press, New York, 333pp.

Greeley, R., Leach, R.N., Williams, S.H., White, B.R., Pollack, J.B., Krinsley, D.H., Marshall, J.R., 1982. Rate of wind abrasion on Mars. J. Geophys. Res. 87, 10,009–10,024.

Greeley, R., Lancaster, N., Lee, S., Thomas, P., 1992. Martian aeolian processes, sediments, and features. In: Kieffer, H.H., Jakosky, B.M., Snyder, C.W., Matthews, M.S. (Eds.), Mars. University of Arizona Press, Tucson, pp. 730–766.

Greeley, R., Bridges, N.T., Kuzmin, R.O., Laity, J.E., 2002. Terrestrial analogs to aeolian features seen from the surface of Mars. J. Geophys. Res. 107, 5-1-5-21.

Hickox, C.F., 1959. Formation of ventifacts in a moist, temperature climate. Bull. Geol. Soc. Amer. 70, 1489–1490.

Higgins, C.G., 1956. Formation of ventifacts in a moist, temperate climate. J. Geol. 64, 506–516.

King, L.C., 1936. Wind-faceted stones from Marlborough. New Zealand. J. Geol. 44, 201–213.

Kuenen, P.H., 1928. Experiments on the formation of wind-worn pebbles. Leische Geol. Melellinger 3, 17–38.

Kuenen, P.H., 1960. Experimental abrasion 4: Eolian action. J. Geol. 68, 427–449.

Laity, J.E., 1992. Ventifact evidence for Holocene wind patterns in the east-central Mojave Desert. Z. Geomorphol. Supl. 84, 1–16.

Laity, J.E., 1994. Landforms of aeolian erosion. In: Abrahams, A.D., Parsons, A.J. (Eds.), Geomorphology of Desert Environments. Chapman and Hall, London.

Laity, J.E., 1995. Wind abrasion and ventifact formation in California. In: Tchakerian (Ed.), Desert Aeolian Processes, Chapman & Hall, London.

Lancaster, N., 1984. Characteristics and occurrence of wind erosion features in the Namib Desert. Earth Surf. Process. Landforms 9, 468–478.

Lancaster, N., Greeley, R., 1990. Sediment volume in the north polar sand seas of Mars. J. Geophys. Res. 95, 10,921–10,927.

Lindsay, J.F., 1973. Ventifact evolution in Wright Valley, Antarctica. Geol. Soc. Amer. Bull. 84, 1791–1798.

Malin, M.C, Edgett, K.S., 2001. Global Surveyor Mars Orbiter Camera: interplanetary cruise through primary mission. J. Geophys. Res. 106, 23,429–23,570.

Maxson, J.H., 1940. Fluting and faceting of rock fragments. J. Geol. 48, 717–751.

McCauley, J.F., Breed, C.S., El-Baz, F., Whitney, M.I., Grolier, M.J., Ward, A.W., 1979. Pitted and fluted rocks in the Western Desert of Egypt: Viking comparison. J. Geophys. Res. 84, 8222–8232.

Mutch, T.A., Arvidson, R.E., Binder, A.B., Guinness, E.A., Morris, E.C., 1977. The geology of the Viking 2 landing site. J. Geophys. Res. 82, 4452–4467.

Raupach, M.R., Gillette, D.A., Leys, J.F., 1993. The effect of roughness elements on wind erosion threshold. J. Geophys. Res. 98, 3023–3029.

Ryan, J.A., Henry, R.M., 1979. Mars atmospheric phenomena during major dust storms, as measured at the surface. J. Geophys. Res. 84, 2821–2829.

Schoewe, W.H., 1932. Experiments on the formation of wind-faceted pebbles. Am. J. Sci. 224, 111–134.

Schofield, J.T., Barnes, J.R., Crisp, D., Haberle, R.M., Larsen, S., Magalhaes, J.A., Murphy, J.R., Seiff, A., Wilson, G., 1997. The Mars Pathfinder atmospheric structure investigation/meteorology (ASI/MET) experiment. Science 278, 1752–1758.

Sharp, R.P., 1949. Pleistocene ventifacts east of the Big Horn Mountains, Wyoming. J. Geol. 57, 175–195.

Sharp, R.P., 1964. Wind-driven sand in Coachella Valley, California. Geol. Soc. Am. Bull. 74, 785–804.

Sharp, R.P., 1980. Wind-driven sand in Coachella Valley, California: further data. Geol. Soc. Am. Bull. 91, 724–730.

Sharp, R.P., Saunders, R.S., 1978. Aeolian activity in westernmost Coachella Valley and at Garnet Hill. In: Greeley, R., Womer, M.B., Papson, R.P., Spudis, P.D. (Eds.), Aeolian features of Southern California: a comparative planetary geology guidebook. U.S. Gov. Printing Office, Washington, pp. 9–22.

Smalley, I.J., Krinsley, D.H., 1979. Eolian sedimentation on Earth and Mars: some comparisons. Icarus 40, 276–288.

Suzuki, T., Takahashi, K., 1981. An experimental study of wind abrasion. J. Geol. 89, 23–36.

Tanaka, K.L., Scott, D.H., Greeley, R., 1992. Global stratigraphy. In: Kieffer, H.H., Jakosky, B.M., Snyder, C.W., Matthews, M.S. (Eds.), Mars. University of Arizona Press, Tucson, pp. 345–382.

Thomas, P.C., Weitz, C., 1989. Sand dune materials and polar layered deposits on Mars. Icarus 81, 185–215.

Viking Lander Team, 1978. The Martian Landscape, NASA Spec. Publ. SP-425, 160pp.

Ward, A.W., 1979. Yardangs on Mars: evidence of recent winds. J. Geophys. Res. 84, 8147–8166.

Wentworth, C.K., Dickey, R.I., 1935. Ventifact localities in the United States. J. Geol. 43, 97–104.

White, B.R., Shulz, J.C., 1977. Magnus effect on saltation. J. Fluid Mech. 81, 497–512.

White, B.R., Greeley, R., Iversen, J.D., Pollack, J.B., 1976. Estimated grain saltation in a Martian atmosphere. J. Geophys. Res. 81, 5643–5650.

Whitney, M.I., 1978. The role of vorticity in developing lineation by wind erosion. Geol. Soc. Am. Bull. 89, 1–18.

Whitney, M.I., Dietrich, R.V., 1973. Ventifact sculpture by windblown dust. GSA. Bull. 84, 2561–2582.

Zimbelman, J.R., 2000. Non-active dunes in the Acheron Fossae region of Mars between the Viking and Mars Global Surveyor era. Geophys. Res. Lett. 27, 1069–1072.